






Novel transient cytoplasmic rings stabilize assembling bacterial flagellar motors

Mohammed Kaplan¹, Catherine M Oikonomou¹ , Cecily R Wood² , Georges Chreifi¹, Poorna Subramanian¹, Davi R Ortega¹, Yi-Wei Chang³ , Morgan Beeby⁴, Carrie L Shaffer^{2,5,6}  & Grant J Jensen^{1,7,*} 

Abstract

The process by which bacterial cells build their intricate flagellar motility apparatuses has long fascinated scientists. Our understanding of this process comes mainly from studies of purified flagella from two species, *Escherichia coli* and *Salmonella enterica*. Here, we used electron cryo-tomography (cryo-ET) to image the assembly of the flagellar motor *in situ* in diverse Proteobacteria: *Hylemonella gracilis*, *Helicobacter pylori*, *Campylobacter jejuni*, *Pseudomonas aeruginosa*, *Pseudomonas fluorescens*, and *Shewanella oneidensis*. Our results reveal the *in situ* structures of flagellar intermediates, beginning with the earliest flagellar type III secretion system core complex (ft3SScc) and MS-ring. In high-torque motors of Beta-, Gamma-, and Epsilon-proteobacteria, we discovered novel cytoplasmic rings that interact with the cytoplasmic torque ring formed by FliG. These rings, associated with the MS-ring, assemble very early and persist until the stators are recruited into their periplasmic ring; in their absence the stator ring does not assemble. By imaging mutants in *Helicobacter pylori*, we found that the ft3SScc proteins FliO and FliQ are required for the assembly of these novel cytoplasmic rings. Our results show that rather than a simple accretion of components, flagellar motor assembly is a dynamic process in which accessory components interact transiently to assist in building the complex nanomachine.

Keywords assembly; bacterial flagellar motor; cryo-ET; high-torque; tomography

Subject Category Microbiology, Virology & Host Pathogen Interaction

DOI 10.15252/emboj.2021109523 | Received 22 August 2021 | Revised 31 January 2022 | Accepted 16 February 2022 | Published online 18 March 2022

The EMBO Journal (2022) 41: e109523

Introduction

Having undergone billions of years of optimization through natural selection, the bacterial flagellum represents a rich system to study how biological nanomachines are assembled at the macromolecular level. A prime example of a multi-component complex that is built through a tightly regulated self-assembly process (Macnab, 2003), the flagellum consists of a long extracellular filament driven by a cell envelope-embedded motor at its base, connected through a flexible joint known as the hook (Fig EV1).

Our current understanding of how this structure assembles is based primarily on the popular model organisms *Escherichia coli* and *Salmonella enterica* (both Gammaproteobacteria). Flagellar biogenesis is believed to proceed in an inside-out fashion (Fig 1), beginning with the assembly of a part of the flagellar type III secretion system (ft3SS) known as the core complex (ft3SScc), an integral inner membrane (IM) complex consisting of five proteins (FliP, FliQ, FliR, FlhB, and FlhA) (Abrusci *et al.*, 2013). A sixth protein, FliO, is believed to be required for the assembly of the ft3SScc but does not form part of the complex (Fabiani *et al.*, 2017; Fukumura *et al.*, 2017). The assembly of the ft3SScc initiates with FliP, which forms a pentameric platform on which FliQ, FliR, and FlhB assemble to create a FliP₅FliQ₄FliR₁FlhB₁ subcomplex upon which a nonameric FlhA ring is built (Fabiani *et al.*, 2017; Kuhlen *et al.*, 2018; Minamino *et al.*, 2019; Milne-Davies *et al.*, 2021). The C-terminal domains of both FlhA and FlhB remain in the cytoplasm (Fig 1, top).

Upon formation of the ft3SScc, the MS-ring (FliF) and C-ring (FliG, FliM, and FliN) assemble, followed by the cytoplasmic ft3SS ATPase (FliH, FliI, and FliJ) inside the C-ring. Biogenesis of the ft3SS promotes secretion of additional periplasmic and extracellular components across the IM including the flagellar rod (FliE, FlgB, FlgC, FlgF, and FlgG), hook (FlgE), hook-filament junction proteins (FlgK and FlgL), filament capping protein (FliD), and filament subunits (FliC) (Macnab, 2003) (Fig 1, bottom). The periplasmic P-ring (FlgI) and L-ring (FlgH) which assemble around the rod are secreted through the IM via the Sec pathway (Macnab, 2003). Additional

¹ Division of Biology and Biological Engineering, California Institute of Technology, Pasadena, CA, USA

² Department of Veterinary Science, University of Kentucky, Lexington, KY, USA

³ Department of Biochemistry and Biophysics, Perelman School of Medicine, University of Pennsylvania, Philadelphia, PA, USA

⁴ Department of Life Sciences, Imperial College London, London, UK

⁵ Department of Microbiology, Immunology, and Molecular Genetics, University of Kentucky, Lexington, KY, USA

⁶ Department of Pharmaceutical Sciences, University of Kentucky, Lexington, KY, USA

⁷ Department of Chemistry and Biochemistry, Brigham Young University, Provo, UT, USA

*Corresponding author. Tel: +626 395 8827; E-mail: jensen@caltech.edu

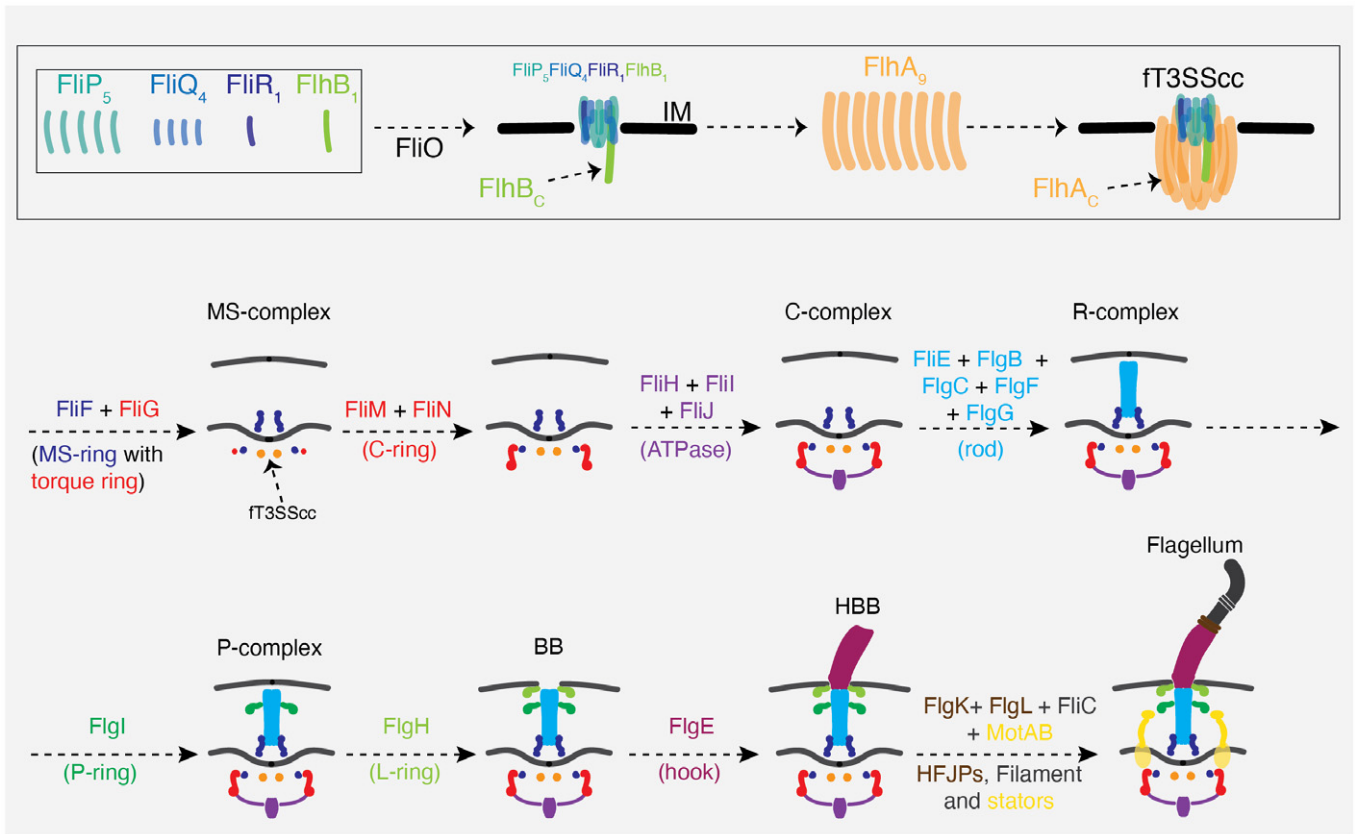


Figure 1. Current understanding of flagellar assembly based on the canonical systems of *Escherichia coli* and *Salmonella enterica*.

A schematic summary of our current understanding of how *E. coli* and *S. enterica* assemble the ft3SScc (top) and flagellum and the various flagellar complexes formed during this process. See also (Jones & Macnab, 1990; Kubori *et al.*, 1992; Macnab, 2003; Li & Sourjik, 2011; Fabiani *et al.*, 2017). The color code for the different parts of the flagellum is used in all subsequent schematics (except Appendix Fig S3), and labels are shown only in some schematics to avoid redundancy. HFJPs = hook-filament junction proteins.

chaperones and capping proteins assist in the assembly process. While all known motors share this conserved core, various embellishments are found in different species, highlighting the continuous evolution of this nanomachine (Chen *et al.*, 2011; Zhao *et al.*, 2014; Qin *et al.*, 2017; Chaban *et al.*, 2018; Kaplan *et al.*, 2019a).

The C-ring, MS-ring, rod, hook, and filament make up the rotor of the motor. Torque is generated by a ring of IM-embedded ion channels known as stators which translate the flux of ions into rotation of the C-ring (also called the torque ring) through interaction with FliG (Chang *et al.*, 2020; Deme *et al.*, 2020; Santiveri *et al.*, 2020). While the majority of motors use H⁺- or Na⁺-dependent stators, others can use different cations (Terahara *et al.*, 2012; Ito & Takahashi, 2017). In addition, stators have also been discovered that can use either Na⁺ or H⁺ in a pH-dependent manner, as well as motors with dual stator systems (Terahara *et al.*, 2008; Thormann & Paulick, 2010). The motors of *E. coli* and *S. enterica* have dynamic stators that continually associate and disassociate from the rotor in response to the external environment (Lele *et al.*, 2013). The motors of some other species generate higher torque with wider, more highly-occupied stator rings stabilized by periplasmic scaffolds and chaperones that directly interact with the stators to maintain their integrity (Beeby *et al.*, 2016; Kaplan *et al.*, 2019a; Ribardo *et al.*, 2019).

The assembly of the flagellum is believed to proceed sequentially, with the addition of each component building upon the previous one (Li & Sourjik, 2011). Additional mechanisms evolved to control the lengths of the different sections of the flagellum. For example, the periplasmic rod (driveshaft) is believed to grow until it hits the outer membrane (OM) (Cohen *et al.*, 2017). FliK is thought to limit the length of the extracellular hook to ~ 50–55 nm (Erhardt *et al.*, 2011; Kodera *et al.*, 2015; Guse *et al.*, 2020). Different models have been proposed for the assembly of the extracellular filament. First, it was proposed that the secreted subunits interact head-to-tail inside the channel of the flagellum and that the folding of subunits at the tip of the growing filament provides a pulling force on the head-to-tail chain (Evans *et al.*, 2013). A more recent model suggests that filament assembly is instead governed by an injection-diffusion mechanism in which the growth kinetics decrease quadratically, thus providing an explanation for why growth does not continue indefinitely (Chen *et al.*, 2017; Hughes, 2017; Renault *et al.*, 2017). For a recent review see (Renault *et al.*, 2019).

Our current understanding of flagellar assembly comes mainly from biochemistry and negative-staining electron microscopy of purified motors, and lower-resolution light microscopy of cells (Jones & Macnab, 1990; Kubori *et al.*, 1992; Li & Sourjik, 2011).

Higher-resolution electron cryo-tomography (cryo-ET) of native motors inside intact cells captured late assembly stages in *Borrelia burgdorferi* (Zhao *et al*, 2013) and non-canonical Gammaproteobacteria (Kaplan *et al*, 2019b), but images of the flagellar assembly process from its earliest stages (the σ T3SScc and the MS-ring) inside the cell are still lacking. Here, we investigated how flagellar motors are built *in situ* using cryo-ET. We identified early flagellar intermediates that precede the formation of the C-ring and rod and discovered that in the absence of the torque ring protein, FliG, the MS-ring does not assemble. Moreover, we identified novel cytoplasmic rings that surround the FliG torque ring during assembly. These ring(s) are built before the C-ring is fully assembled and persist until the stator ring assembles, but are not found in the fully assembled flagellum. By imaging mutants of candidate genes, we discovered that the σ T3SScc proteins FliO and FliQ are required for the formation of the novel cytoplasmic rings.

Results

We identified flagellar motor assembly intermediates in electron cryotomograms of several Proteobacteria species: *Hylemonella gracilis*, *Helicobacter pylori*, *Campylobacter jejuni*, *Shewanella oneidensis*, *Pseudomonas aeruginosa*, and *Pseudomonas fluorescens* (Table EV1). These species have various flagellar arrangements: monotrichous, amphitrichous, and lophotrichous (see Table EV1). For convenience, we refer to flagellar intermediates by the names indicated in Fig 1. In some cases, established terms are available, such as the σ T3SScc, basal body (BB), and hook-basal-body (HBB) complex. For the others, we named them according to either the last component to join the complex or its dominant structural feature. Thus, we have the MS-complex, the C-complex, the R-complex, and the P-complex. Table 1 summarizes the number of examples we identified for each of these complexes in each species. Note that schematics and interpretation of complexes where not enough examples

were found to produce a subtomogram average are tentative. In addition to collecting new cryotomograms for this study, we also mined the Jensen lab tomography database (Ding *et al*, 2015; Ortega *et al*, 2019), which contains more than 40,000 cryotomograms of ~ 90 bacterial species collected in the course of various projects.

Novel transient cytoplasmic rings surround the FliG ring during the assembly of high-torque motors in Beta- and Epsilonproteobacteria

In *Hylemonella gracilis*, a Betaproteobacterium whose thin cells yield high-quality cryo-ET images, we identified eight classes of flagellar motor intermediates corresponding to the MS-complex, the C-complex, the R-complex, the P-complex, BB, HBB, otherwise full flagella lacking the periplasmic collar characteristic of this species (see (Chen *et al*, 2011)), and full flagella with the periplasmic collar (Fig 2 and Movies EV1 and EV2). For many of these classes, we were able to collect enough examples for subtomogram averaging to reveal greater detail (Fig 2A and D, and F–H and Appendix Fig S1). We observed a novel ~55-nm-wide ring located in the cytoplasm 12 nm below the IM (green arrows in Fig 2A–F). This ring was present at the earliest stage of assembly we observed, the MS-complex, and persisted through assembly of the hook. The ring was absent only in the two final complexes where the filament was assembled, either without the periplasmic collar surrounding the P-ring (Fig 2G) or with the collar present and the stators assembled (the fully assembled flagellum) (Fig 2H).

The position of the P-ring in P-complexes was variable (Fig EV2), which explains why the P-ring was not as well-resolved in the subtomogram average of this complex (Fig 2D). We noted that the OM of *H. gracilis* frequently undulates, with the distance between the OM and IM varying significantly around the cell (Fig EV3). Both *S. enterica* and *E. coli* tether their OM to the PG with a protein known as Braun's lipoprotein (Lpp) (Miller & Salama, 2018). The *H. gracilis* genome lacks an Lpp homolog, raising the question of

Table 1. Summary of the number of examples of each flagellar intermediate identified in each species investigated in this study.

Species	No. of tomograms	MS-complex	C-complex	R-complex	P-complex	Basal body	HBB	Motor without collar	Flagellum
<i>Helicobacter pylori</i>	46	11	3	–	–	9	1	–	34
<i>Helicobacter pylori</i> fliP*	76	64	15	–	–	–	–	–	–
<i>H. pylori</i> Δ fliG fliP*	84	21	2	–	–	–	–	–	–
<i>Helicobacter pylori</i> Δ fliM fliP*	265	121	–	–	–	–	–	–	–
<i>Helicobacter pylori</i> Δ fliG fliP*	47	–	–	–	–	–	–	–	–
<i>Helicobacter pylori</i> Δ fliO fliP*	267	47	15	–	–	–	–	–	–
<i>Helicobacter pylori</i> Δ fliQ fliP*	220	94	3	–	–	–	–	–	–
<i>Helicobacter pylori</i> Δ fliF fliP*	455	–	–	–	–	–	–	–	–
<i>Shewanella oneidensis</i> Δ fliG	59	–	–	–	13	–	–	–	–
<i>Campylobacter jejuni</i> Δ fliH _C	19	4	15	–	–	–	–	–	–
<i>Campylobacter jejuni</i> Δ fliA _C	54	8	30	–	–	–	–	–	–
<i>Pseudomonas fluorescens</i>	32	–	–	2	–	2	–	–	4
<i>Hylemonella gracilis</i>	76	5	1	1	35	1	7	8	86

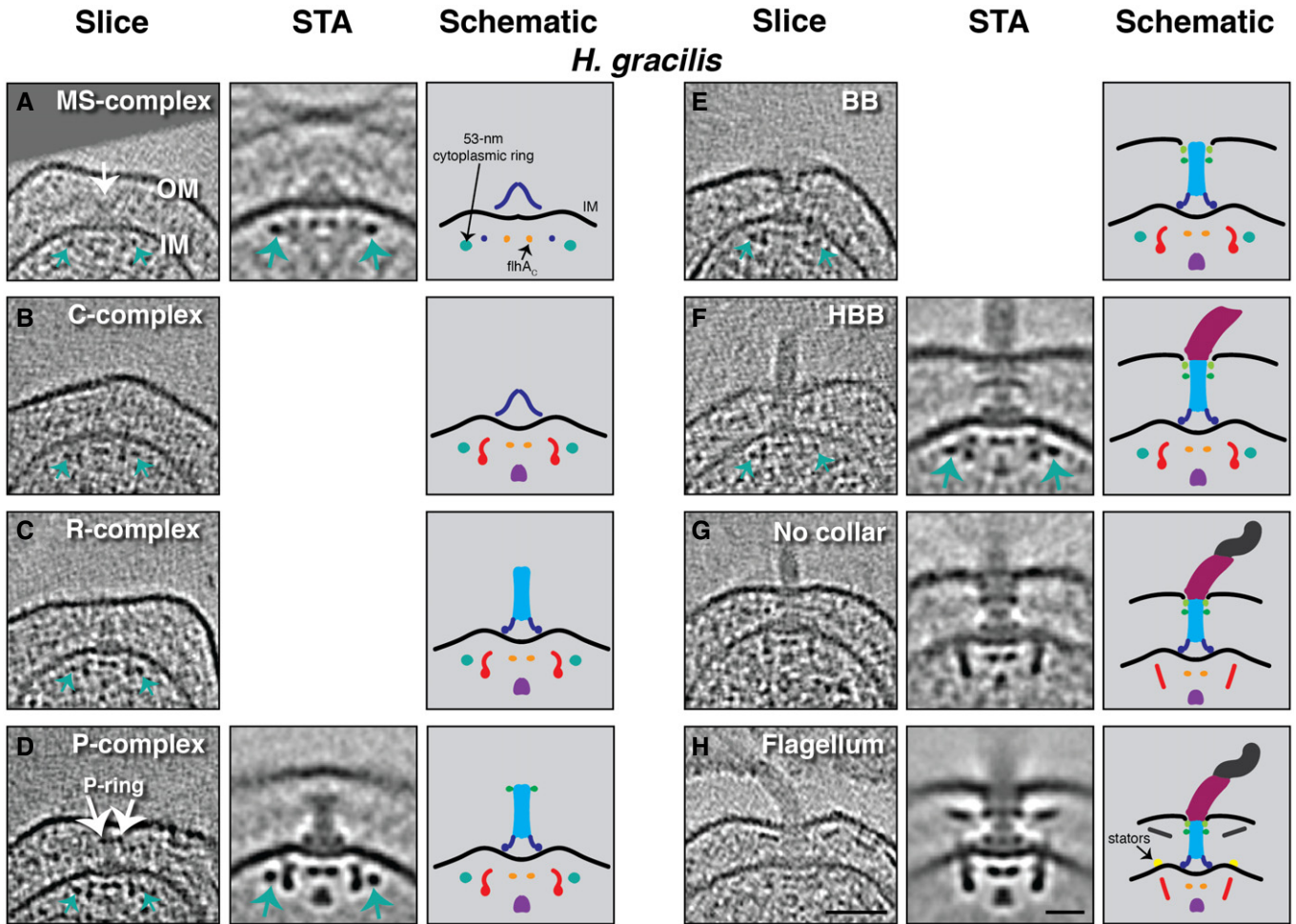


Figure 2. The flagellar assembly pathway of the Betaproteobacterium *Hylemonella gracilis*.

A–H Slices through electron cryotomograms of *H. gracilis* cells (left panels), central slices through subtomogram averages (STA, middle panels), and schematic representations (right panels) representing the various assembly stages observed. White arrow in (A) points to the MS-complex; green arrows point to the novel 55-nm-wide cytoplasmic ring. Scale bars in (H) are 50 nm for the cryotomogram slice and 20 nm for the STA and apply to all panels. Empty panels represent stages where not enough particles were found to produce a STA. OM, outer membrane; IM, inner membrane.

how this bacterium controls its periplasmic space and whether this is related to the variable location of the P-ring. It has recently been shown that some β -barrel proteins can perform the same function as Lpp in some Gram-negative bacteria (Godessart *et al*, 2020; Sandoz *et al*, 2020).

We next examined other high-torque motors, in the Epsilonproteobacteria *Helicobacter pylori* and *Campylobacter jejuni* (Fig EV4). In cryotomograms of *H. pylori*, in addition to fully assembled flagella, we identified the MS-complex, the C-complex, the BB, and the HBB (Fig 3A–D). Interestingly, the MS-complex contained two cytoplasmic rings (one electron-dense and one weaker) surrounding the FlhA_C densities close to the IM, as well as two additional larger cytoplasmic rings with diameters of 58 nm and 75 nm, located 17 nm below the IM (Fig 3A, dark and light green rings). These lower rings were not present at the corresponding position in fully assembled motors (Qin *et al*, 2017) (Fig EV4), or in the BB complex. They were also not readily apparent in cryotomograms of the C-complex, although we did not find enough examples of the complex for

subtomogram averaging to definitively confirm this. In fully assembled *H. pylori* flagella, a periplasmic structure called the cage surrounds the rod and the MS-ring and stabilizes the stator ring (Qin *et al*, 2017). In individual particles, we observed a density that may correspond to the lower part of this cage in the C-complex, suggesting that it is assembled before the rest of the basal body (Fig 3B and Movie EV3).

In a non-motile strain of *H. pylori* which does not produce FlIP due to a naturally occurring point mutation (Chang *et al*, 2018) (henceforth referred to as *flIP**), we identified many MS- and C-complexes (Fig 3E and F and Appendix Fig S2). Subtomogram averaging revealed that these complexes are similar to those in motile cells (Fig 3A–D) but lack the FlhA_C densities (Fig 3E and F). A ring surrounding the MS-ring, previously putatively attributed to FlIL in the fully assembled motor (Qin *et al*, 2017), was seen associated with the MS-complex (Fig 3E). In addition, the entire MS-complex in the *flIP** strain was narrower than in motile cells (Fig 3G and H). For example, the two lower cytoplasmic rings in the *flIP** strain had

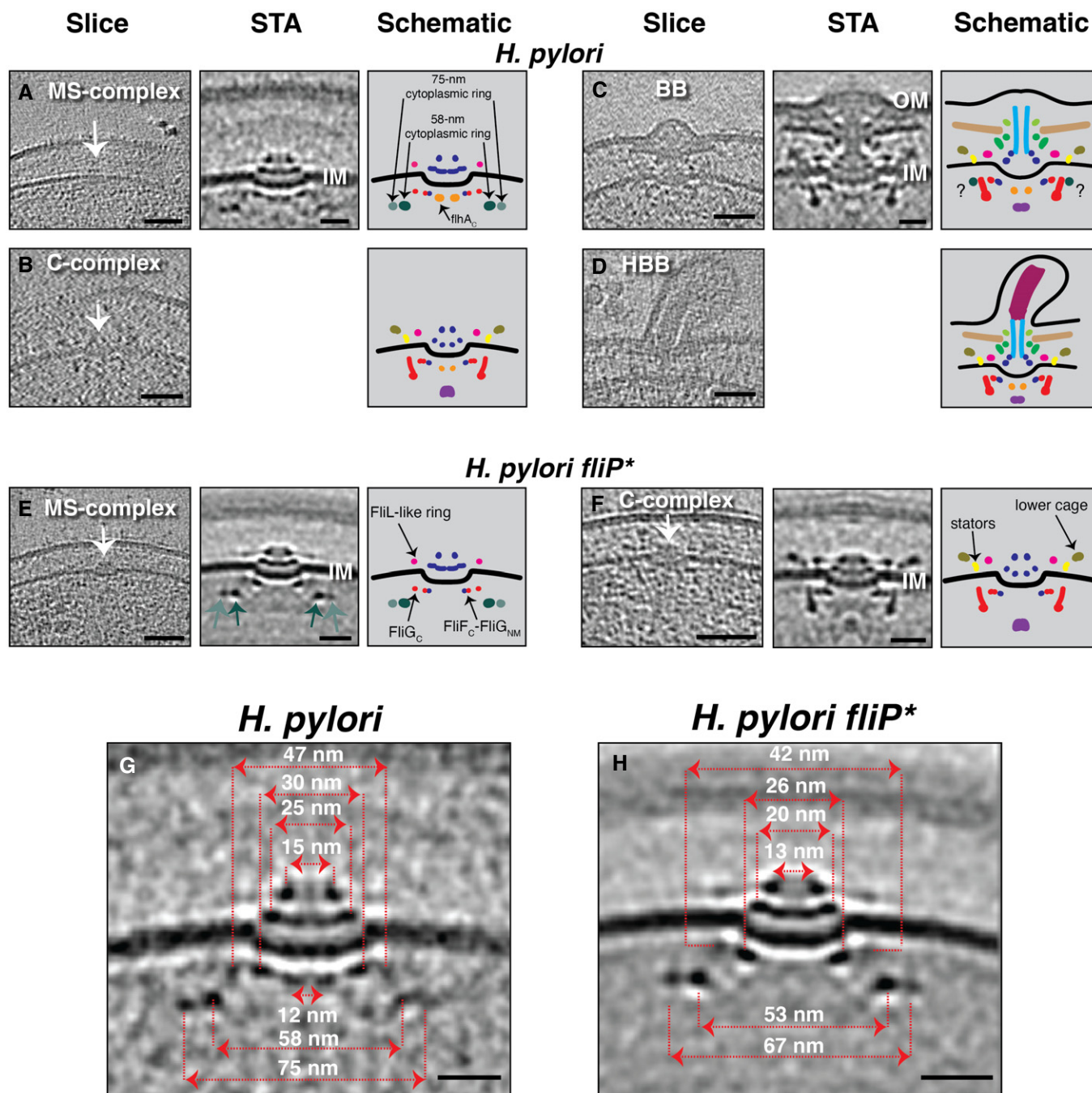


Figure 3. Flagellar assembly intermediates in *Helicobacter pylori*.

A–D Slices through electron cryotomograms of *H. pylori* (left panels) indicating the presence of various flagellar intermediates. Middle panels show central slices through STAs. Right panels show schematic representations. Question marks in the schematic in (C) indicate that it is unclear whether the densities surrounding the upper part of the C-ring are the same as the novel cytoplasmic rings seen in the MS-complex. Empty panels indicate that there were not enough examples to produce a STA.

E, F Cryotomogram slices, STAs, and schematics of *H. pylori fliP** cells showing the MS-complex (E) and the C-complex (F). The two novel cytoplasmic rings are highlighted with light and dark green arrows in the STA panel. White arrows in (A–F) point to the particles.

G, H Central slices through the STAs of the MS-complexes of the motile *H. pylori* (G) and *H. pylori fliP** mutant (H) with the diameters of their various constituent rings indicated.

Data information: Scale bars are 50 nm for cryotomogram slices and 20 nm for STAs.

diameters of 53 and 67 nm, respectively, compared to diameters of 58 and 75 nm in motile cells. A subtomogram average of the C-complex in the *fliP** strain confirmed that the lower cage and the stator ring are assembled at this stage and that the novel cytoplasmic rings are no longer present, or at least not in the same location they occupy in the MS-complex (Fig 3F).

The improved quality of the subtomogram average of the MS-complex in the *fliP** strain allowed us to tentatively assign densities to FliF and FliG (Fig EV5) and compare our structure to available high-resolution structures of the purified MS-ring (Johnson *et al*, 2020; Kawamoto *et al*, 2021). Manually fitting the high-resolution structure of the purified MS-ring from *S. enterica* (PDB 6SCN) (Johnson *et al*, 2020) into the average allowed us to provisionally assign densities to different periplasmic domains including the drive-shaft-housing ring (the Beta collar), the C-ring template (the ring building motif 3 (RBM3) ring), and the RBM2+RBM1 rings. Additionally, fitting the crystal structure of FliG (which is known to interact with FliF) from *Aquifex aeolicus* (PDB 3HJL) (Lee *et al*, 2010) suggested that the dense ring directly surrounding the (here absent) FlhA_C densities probably contains the C terminus of FliF (FliF_C) and the N- and middle domains of FliG (FliG_{MN}), while the peripheral ring contains the C terminus of FliG (FliG_C) (Fig EV5).

We also examined cryotomograms of another Epsilonproteobacterium, *Campylobacter jejuni* (see (Abrusci *et al*, 2013; Beeby *et al*, 2016)). In wild-type *C. jejuni* cells, we found only fully assembled flagella. In mutants lacking the C-terminal domain of either FlhA ($\Delta flhA_C$) or FlhB ($\Delta flhB_C$), however, which do not assemble full flagella, we identified MS- and C-complexes (Fig 4). In the $\Delta flhB_C$ strain, the MS-complex comprised the MS-ring, putative FliG densities, the FT3SScc (as indicated by the presence of the cytoplasmic FlhA_C densities), and, notably, a ~50-nm-wide cytoplasmic ring

located ~17 nm below the IM (as in *H. pylori*) (Fig 4A). The same 50-nm ring was also seen in $\Delta flhA_C$ MS-complexes, which of course lack the cytoplasmic FlhA_C densities (Fig 4C). Neither mutant retained the 50 nm cytoplasmic ring in the C-complex (Fig 4B and D). Fully assembled flagella of *C. jejuni* have two concentric periplasmic discs which assist the assembly of the stator ring (Beeby *et al*, 2016). Similar to the lower portion of the cage in *H. pylori*, we observed these discs in the C-complex of both $\Delta flhB_C$ and $\Delta flhA_C$ cells (Fig 4B and D).

To summarize, we found unexpected cytoplasmic rings encircling the FliG ring in high-torque motors of Betaproteobacteria (*H. gracilis*) and Epsilonproteobacteria (*H. pylori* and *C. jejuni*). These rings assemble very early, associating with the MS-complex before the C-ring is built and then disassemble (or at least do not stay in their original positions) upon addition of the stators and their stabilizing periplasmic scaffolds (assembly stages corresponding to the C-complex in Epsilonproteobacteria and the full flagellum in *H. gracilis*).

The novel rings are dependent on components of the flagellar type III secretion system

In an attempt to identify the protein(s) forming these unexpected cytoplasmic rings, we produced and imaged various mutants in the *H. pylori fliP** background. We chose this strain because: (i) *H. pylori* has multiple polar flagella (up to six per cell); hence, there is a higher chance of identifying flagellar intermediates compared to species with a single flagellum at each pole like *C. jejuni*; (ii) the process of generating mutants is better-established in *H. pylori* than in some other species like *H. gracilis*; and (iii) since *fliP** cells do not proceed to build full flagella, early flagellar assembly stages (like the MS-complex where the novel rings are clearest)

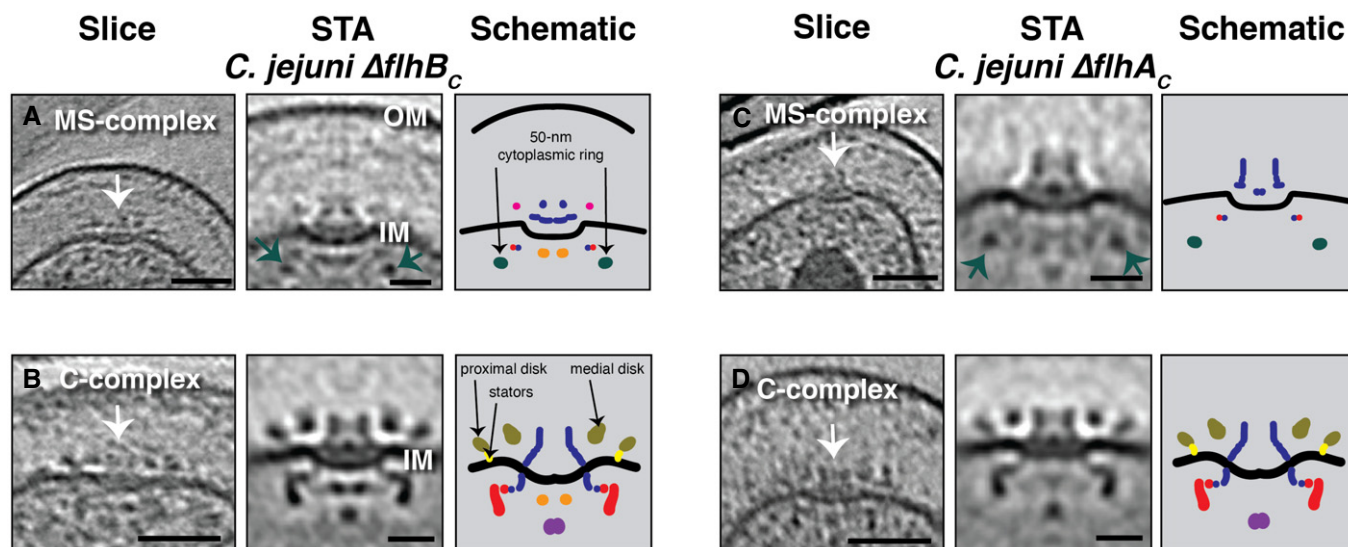


Figure 4. Flagellar intermediates in *Campylobacter jejuni* mutants.

A–D Slices through electron cryotomograms (left panels), central slices through STAs (middle panels), and schematic representations (right panels), of *C. jejuni* $\Delta flhB_C$ and $\Delta flhA_C$ illustrating different flagellar intermediates (highlighted by white arrows). Green arrows in (A) and (C) point to the ~50-nm cytoplasmic ring associated with the MS-complex. Scale bars are 50 nm for cryotomogram slices, 20 nm for STAs.

are abundant. We generated the following mutants in *H. pylori fliP**: $\Delta fliG$, $\Delta fliM$, $\Delta fliG$, $\Delta fliF$, $\Delta fliO$, and $\Delta fliQ$. Despite multiple attempts, we were unable to produce a $\Delta fliR$ mutant.

In contrast to Gammaproteobacteria in which all of the basal body and hook genes belong to the same transcriptional class (Chilcott & Hughes, 2000), in Epsilonproteobacteria genes encoding the basal body are expressed from a hierarchy of two classes, regulated by the cytoplasmic proteins FlgS and FlgR (Gilbreath et al, 2011; Lertsethtakarn et al, 2011) (Appendix Fig S3). FlgS, a sensor kinase that is auto-phosphorylated upon assembly of the FT3SS and the MS- and C-rings (Joslin & Hendrixson, 2009; Lertsethtakarn et al, 2011) (Appendix Fig S3), is required for phosphorylation of FlgR and activation of σ_{54} and σ_{28} , resulting in expression of class II and class III genes, respectively (Lertsethtakarn et al, 2011). We hypothesized that at least one of the novel cytoplasmic rings might

contain FlgS physically interacting with the MS-complex. However, we saw no difference in the MS-complexes present in the $\Delta fliG$ *fliP** strain compared to *fliP** (Fig 5A), nor in two individual examples of the C-complex (Fig 5B and Movie EV4). Also, in Epsilonproteobacteria, the C-ring protein FliM is known to assemble after and interact with, FliG, followed by FliY and then FliN (Henderson et al, 2020). We therefore imaged cells lacking FliM. Again, we saw no difference between the cytoplasmic rings in MS-complexes of $\Delta fliM$ *fliP** and *fliP** strains (Fig 5C and Appendix Fig S4). As expected, no C-complexes were observed in the $\Delta fliM$ strain. We also imaged $\Delta fliG$ *fliP** and $\Delta fliF$ *fliP** strains, but detected no MS- or C-complexes in these two strains despite collecting 47 cryotomograms of $\Delta fliG$ *fliP**, and 455 cryotomograms of $\Delta fliF$ *fliP**.

In addition to these proteins, which we reasoned were likely candidates for the novel cytoplasmic rings, we examined the effect of

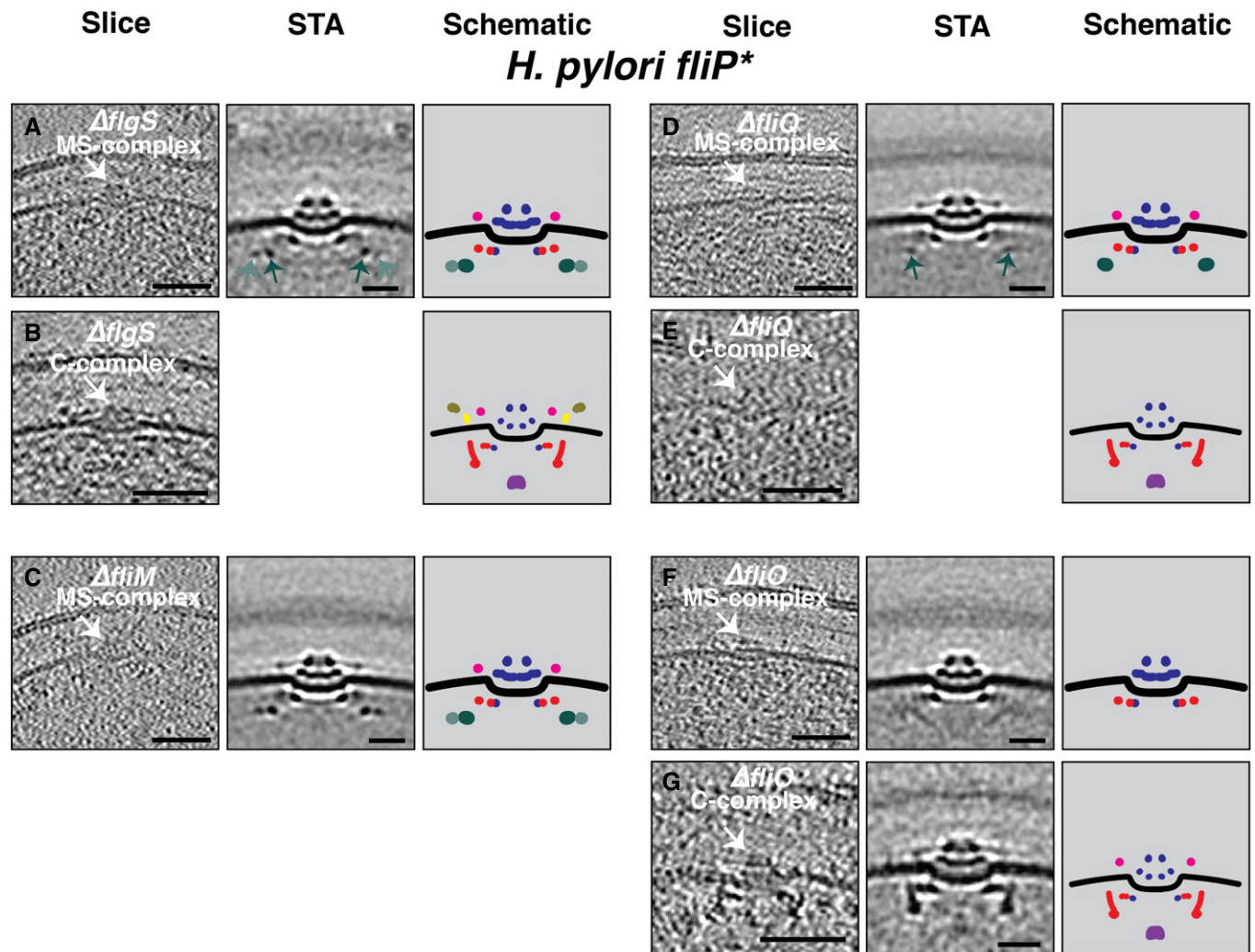


Figure 5. The effect of various mutants on the MS- and C-complexes of *Helicobacter pylori fliP.**

A–G Slices through electron cryotomograms (left panels), central slices of subtomogram averages (middle panels), and schematic representations (right panels) of the MS- and C-complexes (white arrows on the slices) of different mutants in *H. pylori fliP**. Light and dark green arrows in (A and D) point to the ~ 53-nm and ~ 67-nm cytoplasmic rings. Scale bars for cryotomogram slices are 50 nm, and 20 nm for STAs. Empty panels indicate that there were not enough examples to produce a STA.

the two other early-assembling fT3SSc proteins, *fliQ* and *fliO*, on these early flagellar assembly complexes. *FliQ* is a transmembrane protein and is one of the first fT3SSc components to assemble as part of the $\text{FliP}_5\text{FliQ}_4\text{FliR}_1$ subcomplex (Minamino *et al.*, 2019). In $\Delta\text{fliQ fliP}^*$ cells, the MS-complex contained the periplasmic putative *FliL* ring and the 53-nm cytoplasmic ring, but lacked the 67-nm ring (Fig 5D and Appendix Fig S5). Putative C-complexes in $\Delta\text{fliQ fliP}^*$ cells additionally lacked the lower part of the cage and the stators normally present at this stage (Fig 5E and Movie EV5), although not enough examples were identified to produce a subtomogram average (see Table 1). *FliO* is required for assembly of the fT3SSc , but is not thought to form part of the complex (Fabiani *et al.*, 2017; Fukumura *et al.*, 2017). Interestingly, in $\Delta\text{fliO fliP}^*$ cells, both the 53-nm and 67-nm cytoplasmic rings were missing in the MS-complex (Fig 5F), and the C-complex again lacked the lower cage and the stators (Fig 5G). Nonetheless, some faint, angled densities were present in the MS-complex in this mutant, in the location where the novel rings would otherwise appear (Fig 5F, middle panel).

These results show that without either the 67-nm ring ($\Delta\text{fliQ fliP}^*$) or both cytoplasmic rings ($\Delta\text{fliO fliP}^*$), the stator ring and associated stabilizing structures (lower cage) do not assemble.

The novel rings induce a conformational change in the *FliG* torque ring

The fact that the novel cytoplasmic rings are assembled before the full C-ring (in the MS-complex) and are present in flagellar intermediates lacking the cytoplasmic part of the *flhA_C* protein (in *fliP}^** *H. pylori* and ΔflhA_C *C. jejuni* cells) suggests that they interact with *FliG_C*, which is the only other part of the MS-complex accessible to the cytoplasm. To investigate this further, we compared our best subtomogram averages (containing the most particles) of assembly intermediates with and without the novel rings. We first compared the average of the P-complex (with the 55-nm ring) to that of the fully assembled flagellum of *H. gracilis* and observed that the upper part of the C-ring (occupied by *FliG*) was pushed inward in the presence of the cytoplasmic ring (Fig 6A). We then compared the MS-complexes of $\Delta\text{fliM fliP}^*$ (with 53-nm and 67-nm rings present) and $\Delta\text{fliO fliP}^*$ (both rings absent) *H. pylori* and found that the *FliG_C* density was pushed upward (closer to the IM) and outward in the presence of the rings (Fig 6B). These results indicate that the novel cytoplasmic rings interact with and alter the position of, *FliG_C*.

The novel rings are also present in Gammaproteobacteria motors with a stabilized stator ring

We next investigated whether the novel cytoplasmic rings are present in flagellar motors of other classes of bacteria with a stable stator ring. We first examined the motor of *Shewanella oneidensis*, which as in *Vibrio* species, is characterized by periplasmic structures (the H- and T-rings) that stabilize the stator ring (Kaplan *et al.*, 2019a) (Fig EV4D). In cryotomograms of wild-type cells, we observed abundant fully assembled flagella, but few intermediates. This could be due either to the growth conditions used or to the fact that HBB genes are clustered in a single transcriptional class, perhaps rendering their assembly faster than in Epsilonproteobacteria motors. To arrest the process, we imaged *S. oneidensis AflgH* which lacks the L-ring protein *FlgH* and halts assembly at the P-complex.

In electron cryotomograms of this strain, we observed that the P-complex showed a clear ~55-nm cytoplasmic ring surrounding the upper part of the C-ring occupied by *FliG* (Fig 7A).

We next explored *Pseudomonas* spp. While our cryotomograms of wild-type *P. aeruginosa* contained predominantly fully assembled flagella, previous work from another group reported the structure of the C-complex (Zhu *et al.*, 2019). Examining that structure, we noticed an ~56–57-nm cytoplasmic ring surrounding the *FliG* densities in the C-ring (Appendix Fig S6). No comment was made about this ring in the publication. In cryotomograms from the Jensen lab database of *Pseudomonas fluorescens*, which has a motor similar to that of *P. aeruginosa* (Fig EV4E–G), we also found a ~55-nm cytoplasmic ring in the R-complex (Fig 7B).

Together, these results indicate that Gammaproteobacteria motors with a stabilized stator ring also contain an ~55-nm cytoplasmic ring surrounding the *FliG* ring during their assembly, suggesting a common regulatory mechanism for high-torque motors that contain periplasmic scaffolds stabilizing their stator rings. We summarize our findings from Beta-, Gamma-, and Epsilonproteobacteria in Fig 8.

Discussion

Here, we imaged flagellar assembly *in situ* using cryo-ET in diverse bacterial species with high-torque motors (i.e., species that use periplasmic scaffolds to stabilize the stator ring). We discovered cytoplasmic rings encircling the *FliG* torque ring that persists until the stators and their stabilizing structures are assembled. These novel rings likely interact with *FliG*, as its conformation is changed in their presence. We identified these cytoplasmic rings in *H. gracilis*, *H. pylori*, *C. jejuni*, *P. aeruginosa*, *P. fluorescens*, and *S. oneidensis*, representing Beta-, Gamma-, and Epsilonproteobacteria. By imaging various mutants in the *H. pylori fliP}^** background, we showed that the rings (at least in this species) were dependent on *FliO* and *FliQ*, with the outermost ring disappearing in a $\Delta\text{fliQ fliP}^*$ mutant and both rings disappearing in a $\Delta\text{fliO fliP}^*$ mutant. As both *FliO* and *FliQ* are transmembrane proteins, we postulate that these fT3SSc proteins are involved in regulating other proteins that form (or are required to form) the rings, rather than forming the rings directly. Previous biochemical studies have indicated a regulatory role for *FliO* in *H. pylori*, where it is required for the optimal expression of other flagellar genes (Tsang & Hoover, 2014). However, direct physical involvement of these proteins in the formation of the novel cytoplasmic rings cannot be totally excluded.

An important observation is that these cytoplasmic rings persisted until the stators and their stabilizing periplasmic scaffolds assembled. For example, while *C. jejuni* and *H. pylori* lacked the novel cytoplasmic rings in the C-complex (where the stators and the stabilizing lower cage are already assembled), the rings persisted through later stages in *H. gracilis* and *S. oneidensis*, where the periplasmic scaffolds that stabilize the stators are also assembled later. Moreover, the $\Delta\text{fliQ fliP}^*$ and $\Delta\text{fliO fliP}^*$ *H. pylori* mutants, which did not assemble the novel cytoplasmic rings, were also unable to assemble the stators and the lower cage. Nonetheless, the rest of the C-ring proteins could still assemble in these mutants, indicating that the interaction between *FliG* and the subsequently added C-ring

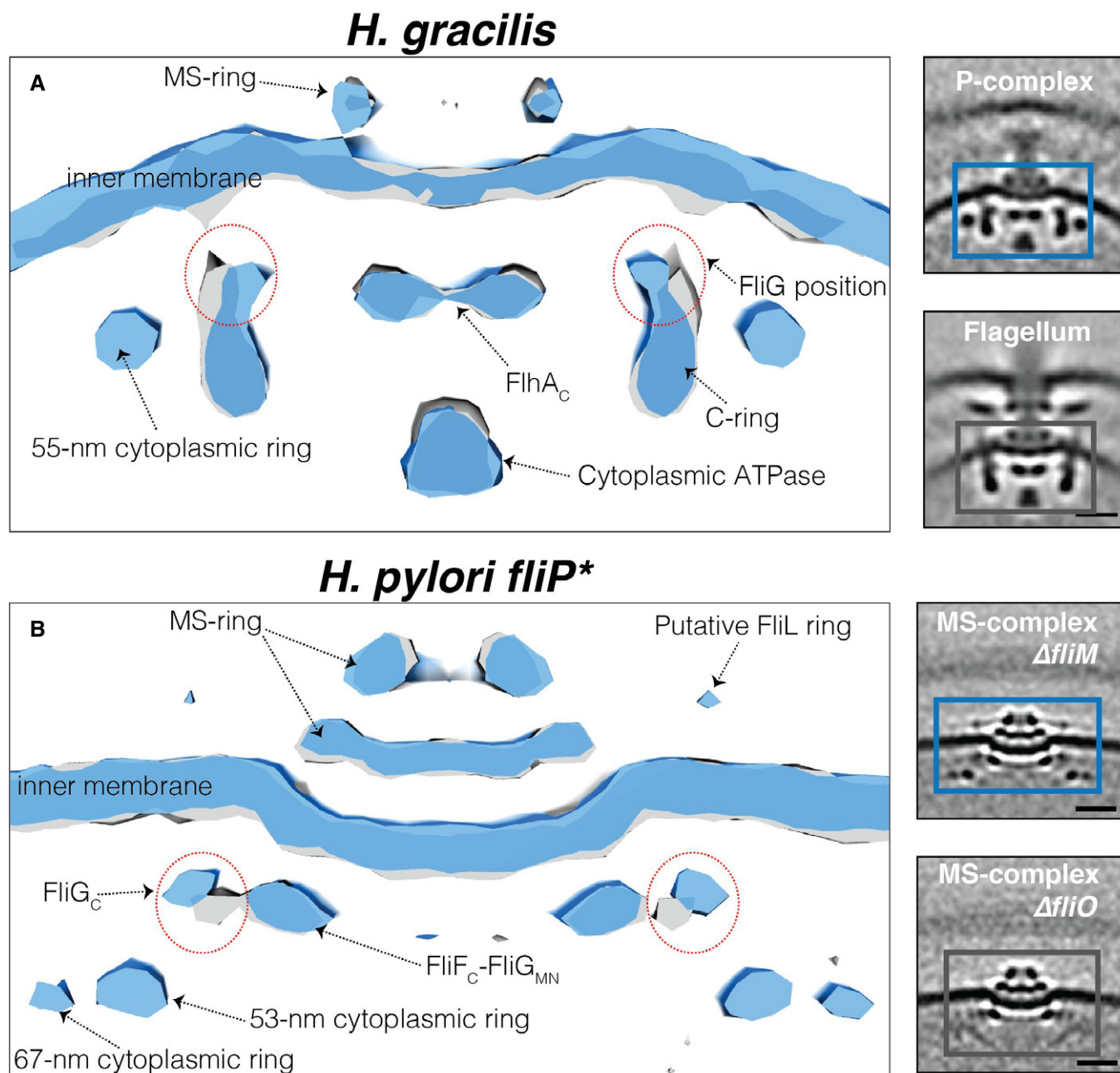


Figure 6. The novel cytoplasmic rings affect the position of the torque ring protein FliG.

A, B Surface renderings of the motor of the fully assembled flagellum (grey) and the P-complex (blue) of *H. gracilis* (A), and the MS-complex of $\Delta fliM \Delta fliP^*$ (blue) and $\Delta fliO \Delta fliP^*$ in *H. pylori* (grey) (B). Boxed areas in the STAs shown on the right represent the surface-rendered areas shown on the left. Red dotted circles in the left panels highlight the different orientations of the FliG protein in these structures. Scale bar is 20 nm.

protein FliM (which interacts with a different part of FliG than the stators (Brown, 2002)) is not affected by the presence/absence of the novel cytoplasmic rings. Taken together, these observations suggest that the interaction between FliG and the surrounding cytoplasmic rings is required for the assembly of the stator ring.

It is possible that these rings lock FliG in a certain conformation that stabilizes the stators before other periplasmic scaffolds are built in high-torque motors. Previous studies on the motor of *S. enterica*,

which does not have a fixed stator ring but rather a variable number of stators depending on the external environment, did not report these rings (Kubori *et al*, 1992). This could be either because the novel rings are found only in high-torque motors with a stable stator ring and absent in *E. coli* and *S. enterica*, or because they were lost in purification of assembly intermediates in *S. enterica*.

It was recently shown that the chemotaxis response regulator CheY interacts with the C-ring of fully assembled flagella, forming

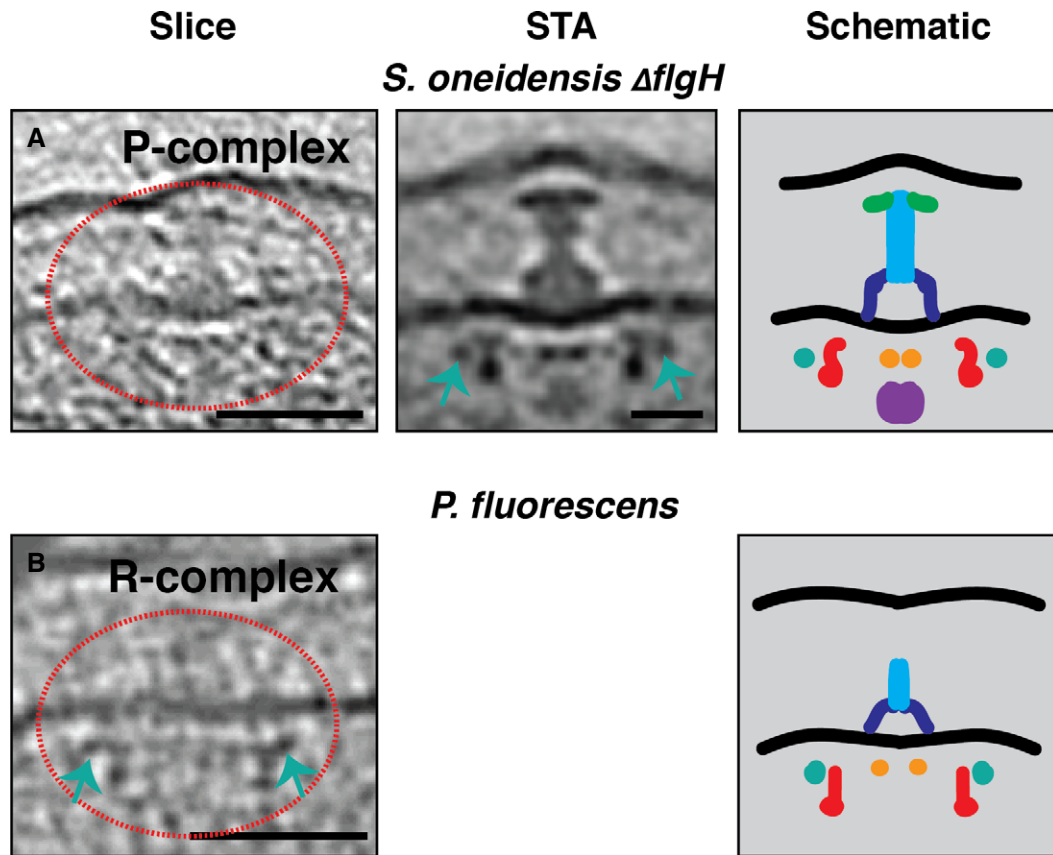


Figure 7. The novel cytoplasmic rings are associated with the assembly of Gammaproteobacteria motors with a stabilized stator ring.

A, B Slices through electron cryotomograms (left panels), central slices through STAs (middle panels), and schematic representations (right panels) of *S. oneidensis* $\Delta flgH$ and *P. fluorescens* illustrating the presence of the ~55-nm cytoplasmic rings during the assembly of these motors (green arrows). Red dotted circles highlight the complexes in the cryotomogram slices. Scale bars are 50 nm for cryotomogram slices, 20 nm for the STA.

an associated ring ~50 nm in diameter that locks the switch complex in clockwise direction by interacting with the C-ring protein FliM (Carroll *et al*, 2020; Chang *et al*, 2020; Rossmann *et al*, 2020). While superficially similar, the novel rings we discovered assemble before FliM and even in its absence (in $\Delta fliM$ *fliP** *H. pylori*), indicating that they are of a different nature.

Recently, Johnson *et al* (2021), Yamaguchi *et al* (2021), and Tan *et al* (2021) reported the molecular structures of the flagellar P- and L-rings from *S. enterica*. Johnson and colleagues observed an outer ring formed by a protein called YecR surrounding the L-ring in their structure, which they hypothesized helps to remodel the lipid bilayer around the L-ring protein, thereby facilitating its assembly in the OM. However, such a ring was not present in the structures solved by Yamaguchi *et al* and Tan and colleagues. Interestingly, while Johnson *et al* purified their particles from a mutant that halts flagellar assembly at the BB stage (lacking the hook protein), Yamaguchi *et al* and Tan *et al* purified their particles from a mutant that proceeds to make the HBB (lacking the filament protein). Our discovery here that transient components are stably present only at certain assembly stages of the flagellar motor and disappear at later stages might explain this difference. It is plausible that the YecR ring is similarly a transient component that helps the assembly of the L-

ring in *S. enterica* and disassembles after the hook is built. Alternatively, of course, differences in the purification protocols used in these studies might have affected the stability of the YecR ring.

The evolutionary history of macromolecular complexes, including the bacterial flagellum, is reflected in their assembly pathways (Liu & Ochman, 2007; Ghosal *et al*, 2019; Beeby *et al*, 2020). In our cryotomograms, FliG was always associated with the MS-ring and we failed to identify any MS-related complexes in $\Delta fliG$ *fliP** mutants, suggesting that FliG is essential for the assembly of the MS-ring, in agreement with previous studies (Li & Sourjik, 2011; Terashima *et al*, 2020). On the other hand, we found that the MS-complex and the novel cytoplasmic rings can still assemble in mutants without a fully assembled $\Delta ft3SScc$, simply adopting a smaller diameter. This ability of the MS-ring to assemble independently of a fully assembled $\Delta ft3SScc$ in these mutants raises the question of how FliF finds and assembles around the $\Delta ft3SScc$ in wild-type cells. Recently, it has been suggested that the absence of the $\Delta ft3SScc$ might result in rings with lower symmetry in the closely related injectisome (Butan *et al*, 2019), and this notion has been used to explain the ability of FliF to form rings with different symmetries *in vitro* (Johnson *et al*, 2020). Similarly, we found that all cytoplasmic and periplasmic components of the C-complex,

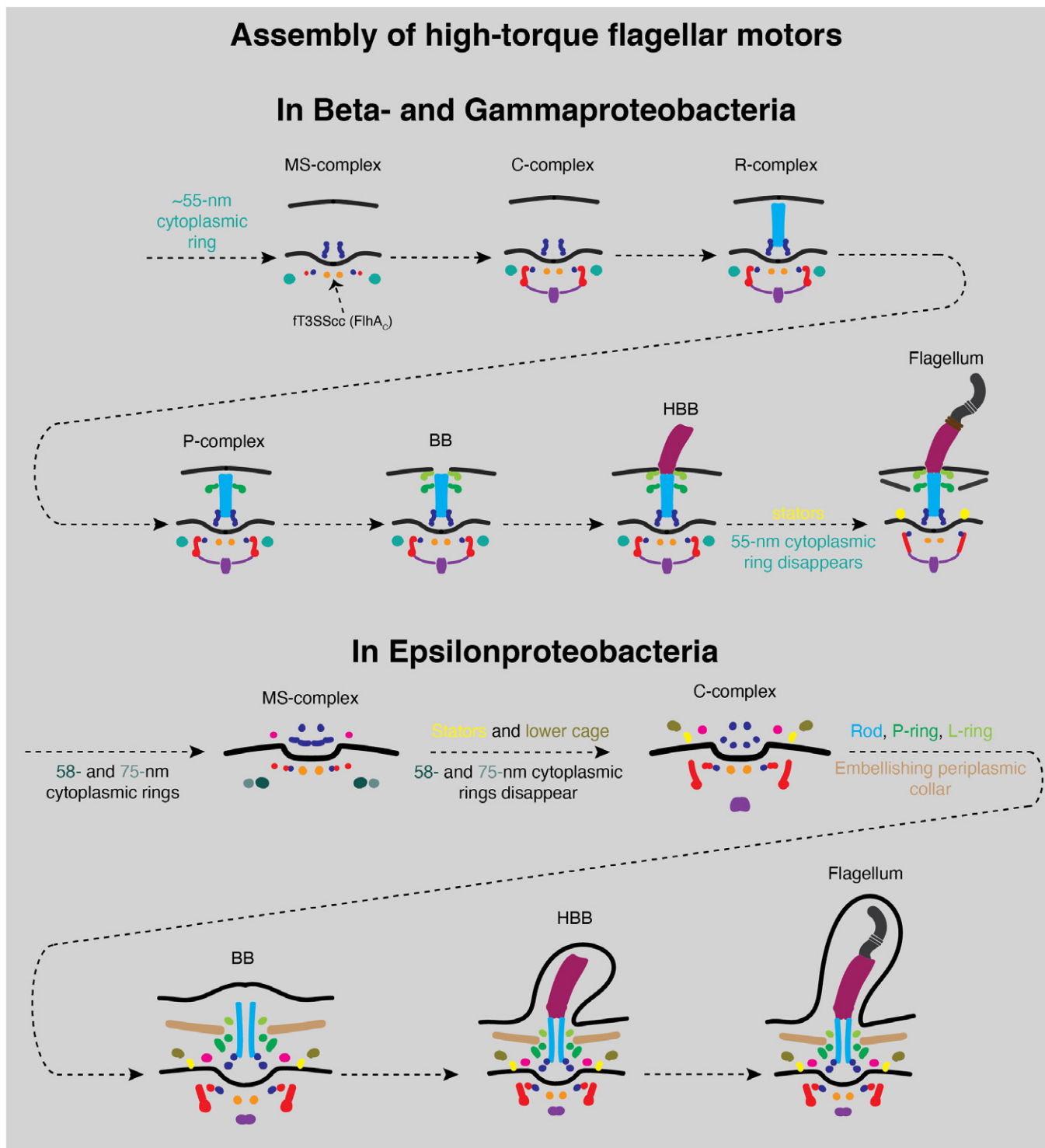


Figure 8. Model of how high-torque motors are built based on *in situ* cryo-ET data.

A schematic summary of our cryo-ET imaging results illustrating how the high-torque motors of Beta-, Gamma-, (top) and Epsilonproteobacteria (bottom) are assembled.

including the cytoplasmic ATPase and the stators with their stabilizing scaffolds, can assemble in the absence of a functional ft3SScc in *H. pylori*. The independent modular assembly of these components

might be a vestige of different evolutionary pasts of these proteins before they combined to produce a new hybrid complex performing a novel motility function.

Materials and Methods

Strains and growth conditions

Pseudomonas fluorescens were grown in K10 medium as detailed in (Boyd *et al*, 2014). *H. gracilis* were grown as described in (Briegel *et al*, 2009; Chen *et al*, 2011; Kaplan *et al*, 2020). Wild-type *C. jejuni* and mutants were grown as described in (Abrusci *et al*, 2013; Beeby *et al*, 2016). *S. oneidensis* Δ flgH were prepared as described in (Kaplan *et al*, 2019b) and grown aerobically in LB culture at 30°C with shaking at 175 rpm to OD₆₀₀ 2.4–2.8.

A motile revertant *H. pylori* 26695 isolate was selected by serial passage in Brucella broth supplemented with 10% heat-inactivated fetal bovine serum at 37°C, 5% CO₂ for 4 days until cultures reached an OD₆₀₀ ~ 0.4. Non-motile *H. pylori* *fliP** mutants were propagated on TSAII blood agar plates (BD Biosciences) at 37°C, 5% CO₂ for either 24 or 48 h prior to collection with a sterile cotton swab for grid preparation.

Helicobacter pylori mutants (Δ fliM *fliP**, Δ fliO *fliP**, Δ fliG *fliP**, Δ fliQ *fliP**, Δ fliF *fliP**) were grown directly from glycerol stocks on sheep blood agar at 37°C with 5% CO₂ for 48 h. Then, the cells were either collected from the plate using a cotton swab and dissolved in PBS and spun down and plunge-frozen directly or the cells were spread on a new plate and allowed to grow for 24 h under the same conditions before plunge-freezing. No difference could be discerned between the two samples by cryo-ET.

Helicobacter pylori mutagenesis

Flagellar mutants were generated in the non-motile *H. pylori* 26695 background as previously described (Shaffer *et al*, 2011). Briefly, constructs were generated to replace the coding region of the gene of interest with an in-frame, non-polar kanamycin resistance cassette. The target gene and approximately 500 base pairs (bp) upstream and downstream of flanking regions were amplified and cloned into pGEM T-Easy (Promega). This construct was used as a template for inverse PCR to remove the majority of the target gene coding region and to introduce incompatible restriction sites for directional cloning. A kanamycin resistance cassette driven by a promoter transcribed in the same direction as the endogenous operon was cloned into the ligated inverse PCR plasmid. *H. pylori* 26695 was transformed via natural competence, and single colonies resistant to kanamycin (12.5 µg/ml) were selected. PCR was used to verify that the kanamycin resistance cassette had inserted into the target locus in the same orientation as operon transcription.

Cryo-ET sample preparation and imaging

R2/2 carbon-coated 200 mesh copper Quantifoil grids (Quantifoil Micro Tools) were glow-discharged for 60 s. Then, cells were mixed with BSA-treated 10- or 20-nm gold solution. 4 µl of this mixture was applied on the grids in a Vitrobot chamber (FEI). Subsequently, the extra fluid was blotted off using a Whatman filter paper in the Vitrobot chamber with 100% humidity and the grids were plunge-frozen in a liquid ethane/propane mixture. Cells were then imaged using either an FEI Polara 300 keV field emission gun electron

microscope (FEI company, Hillsboro, OR, USA) equipped with a Gatan image filter and K2 Summit direct electron detector in counting mode (Gatan, Pleasanton, CA, USA), or a Titan Krios 300 keV field emission gun transmission electron microscope (Thermo Fisher Scientific) equipped with a Gatan imaging filter and a K2 Summit direct detector in counting mode (Gatan). Data were collected using either the UCSF Tomography software (Zheng *et al*, 2007) or SerialEM (Mastrorarde, 2005), with each tilt series ranging from –60° to 60° in 1°, 2° or 3° increments, and an underfocus of ~ 5–10 µm.

The majority of *H. pylori* mutants were imaged using the fast-incremental single exposure (FISE) method (Chreifi *et al*, 2019; Eisenstein *et al*, 2019) with SerialEM software (Mastrorarde, 2005), using a dose-symmetric tilt scheme adapted from Hagen *et al* (2017), a tilt range of –60° to +60°, 3° tilt increment, target defocus of –6 µm, pixel size of 4.49 Å, frame rate of 0.05 s/frame, and a total dose of 130 e⁻/Å². FISE tilt-series were gain normalized and motion-corrected using IMOD's alignframes (Kremer *et al*, 1996).

Cumulative electron doses used for each individual tilt series are shown in Table EV1.

Image processing and subtomogram averaging

Three-dimensional reconstructions of tilt-series were performed either automatically through the RAPTOR pipeline used in the Jensen lab (Ding *et al*, 2015) or with the IMOD software package (Kremer *et al*, 1996). The PEET program (Nicastro, 2006) was used to produce sub-tomogram averages with 2-fold symmetrization along the particle Y-axis. Surface renderings were visualized in Chimera (Pettersen *et al*, 2004). The number of particles that were averaged is listed in the table below:

Figure	Number of particles
Fig 2A	5
Fig 2D	35
Fig 2F	7
Fig 2G	8
Fig 2H	86
Fig 3A	10
Fig 3C	8
Fig 3E	64
Fig 3F	15
Fig 4A	4
Fig 4B	15
Fig 4C	8
Fig 4D	30
Fig 5A	21
Fig 5C	121
Fig 5D	94
Fig 5F	47
Fig 5G	15
Fig 7A	13

Data availability

The following subtomogram averages have been deposited in the Electron Microscopy Data Bank (<https://www.ebi.ac.uk/emdb/>) under the following accession codes: fully assembled flagellar motor of *H. gracilis* (EMD-25702; <https://www.ebi.ac.uk/emdb/EMD-25702>), the MS-complex of *H. pylori* Δ *fliM fliP** (EMD-25703; <http://www.ebi.ac.uk/pdbe/entry/EMD-25703>), the MS-complex of *H. pylori* *fliP** (EMD-25704; <http://www.ebi.ac.uk/pdbe/entry/EMD-25704>), the MS-complex of *H. pylori* Δ *fliQ fliP** (EMD-25705; <http://www.ebi.ac.uk/pdbe/entry/EMD-25705>).

Expanded View for this article is available online.

Acknowledgements

This project was funded by the NIH (grant R01 AI127401 to G.J.J and NIH P20 GM130456 to C.L.S.) and a Baxter postdoctoral fellowship from Caltech to M.K. Cryo-ET work was performed in the Beckman Institute Resource Center for Transmission Electron Microscopy at the California Institute of Technology. We are grateful to Prof. Marc Erhardt (Humboldt-Universität zu Berlin) for critically reading an initial version of this work.

Author contributions

Grant J Jensen: Conceptualization; Resources; Formal analysis; Funding acquisition; Writing—review and editing. **Mohammed Kaplan:** Conceptualization; Data curation; Formal analysis; Funding acquisition; Investigation; Methodology; Writing—original draft; Writing—review and editing. **Catherine M Oikonomou:** Formal analysis; Writing—review and editing. **Cecily R Wood:** Data curation; Methodology; Writing—review and editing. **Georges Chreifi:** Data curation; Writing—review and editing. **Poorna Subramanian:** Data curation; Writing—review and editing. **Davi R Ortega:** Data curation; Writing—review & editing. **Yi-Wei Chang:** Data curation; Writing—review and editing. **Morgan Beeby:** Data curation; Writing—review and editing. **Carrie Shaffer:** Data curation; Funding acquisition; Methodology; Writing—review and editing.

In addition to the CRediT author contributions listed above, the contributions in detail are:

MK and GJJ designed research. MK, CRW, PS, YWC, MB, and CLS prepared samples. MK, GC, PS, YWC, and MB collected data. MK, CMO, DRO, CLS, and GJJ analyzed data. MK wrote the manuscript and all authors edited it.

Disclosure and competing interests statement

The authors declare that they have no conflict of interest.

References

- Abrusci P, Vergara-Irigaray M, Johnson S, Beeby MD, Hendrixson DR, Roversi P, Friede ME, Deane JE, Jensen GJ, Tang CM *et al* (2013) Architecture of the major component of the type III secretion system export apparatus. *Nat Struct Mol Biol* 20: 99–104
- Beeby M, Ferreira JL, Tripp P, Albers S-V, Mitchell DR (2020) Propulsive nanomachines: the convergent evolution of archaella, flagella and cilia. *FEMS Microbiol Rev* 44: 253–304
- Beeby M, Ribardo DA, Brennan CA, Ruby EG, Jensen GJ, Hendrixson DR (2016) Diverse high-torque bacterial flagellar motors assemble wider stator rings using a conserved protein scaffold. *Proc Natl Acad Sci U S A* 113: E1917–E1926
- Boyd CD, Smith TJ, El-Kirat-Chatel S, Newell PD, Dufrene YF, O'Toole GA (2014) Structural features of the pseudomonas fluorescens biofilm adhesin LapA required for LapC-dependent cleavage, biofilm formation, and cell surface localization. *J Bacteriol* 196: 2775–2788
- Briegel A, Ortega DR, Tocheva EI, Wuichet K, Li Z, Chen S, Müller A, Iancu CV, Murphy GE, Dobro MJ *et al* (2009) Universal architecture of bacterial chemoreceptor arrays. *Proc Natl Acad Sci U S A* 106: 17181–17186
- Brown PN (2002) Crystal structure of the middle and C-terminal domains of the flagellar rotor protein FliG. *The EMBO Journal* 21: 3225–3234
- Butan C, Lara-Tejero M, Li W, Liu J, Galán JE (2019) High-resolution view of the type III secretion export apparatus in situ reveals membrane remodeling and a secretion pathway. *Proc Natl Acad Sci U S A* 116: 24786–24795
- Carroll BL, Nishikino T, Guo W, Zhu S, Kojima S, Homma M, Liu J (2020) The flagellar motor of *Vibrio alginolyticus* undergoes major structural remodeling during rotational switching. *eLife* 9: e61446
- Chaban B, Coleman I, Beeby M (2018) Evolution of higher torque in Campylobacter-type bacterial flagellar motors. *Sci Rep* 8: 97
- Chang Y-W, Shaffer CL, Rettberg LA, Ghosal D, Jensen GJ (2018) *In vivo* structures of the *Helicobacter pylori* cag Type IV secretion system. *Cell Rep* 23: 673–681
- Chang Y, Zhang K, Carroll BL, Zhao X, Charon NW, Norris SJ, Motaleb MA, Li C, Liu J (2020) Molecular mechanism for rotational switching of the bacterial flagellar motor. *Nat Struct Mol Biol* 27: 1041–1047
- Chen M, Zhao Z, Yang J, Peng K, Baker MA, Bai F, Lo C-J (2017) Length-dependent flagellar growth of *Vibrio alginolyticus* revealed by real time fluorescent imaging. *eLife* 6: e22140
- Chen S, Beeby M, Murphy GE, Leadbetter JR, Hendrixson DR, Briegel A, Li Z, Shi J, Tocheva EI, Müller A *et al* (2011) Structural diversity of bacterial flagellar motors: Structural diversity of bacterial flagellar motors. *EMBO J* 30: 2972–2981
- Chilcott GS, Hughes KT (2000) Coupling of flagellar gene expression to flagellar assembly in *Salmonella enterica* serovar typhimurium and *Escherichia coli*. *Microbiol Mol Biol Rev* 64: 694–708
- Chreifi G, Chen S, Metskas LA, Kaplan M, Jensen GJ (2019) Rapid tilt-series acquisition for electron cryotomography. *J Struct Biol* 205: 163–169
- Cohen EJ, Ferreira JL, Ladinsky MS, Beeby M, Hughes KT (2017) Nanoscale-length control of the flagellar driveshaft requires hitting the tethered outer membrane. *Science* 356: 197–200
- Deme JC, Johnson S, Vickery O, Aron A, Monkhouse H, Griffiths T, James RH, Berks BC, Coulton JW, Stansfeld PJ *et al* (2020) Structures of the stator complex that drives rotation of the bacterial flagellum. *Nat Microbiol* 5: 1553–1564
- Ding HJ, Oikonomou CM, Jensen GJ (2015) The caltech tomography database and automatic processing pipeline. *J Struct Biol* 192: 279–286
- Eisenstein F, Danev R, Pilhofer M (2019) Improved applicability and robustness of fast cryo-electron tomography data acquisition. *J Struct Biol* 208: 107–114
- Erhardt M, Singer HM, Wee DH, Keener JP, Hughes KT (2011) An infrequent molecular ruler controls flagellar hook length in *Salmonella enterica*: Infrequent molecular ruler controls flagellar hook length in *S. enterica*. *EMBO J* 30: 2948–2961
- Evans LDB, Poulter S, Terentjev EM, Hughes C, Fraser GM (2013) A chain mechanism for flagellum growth. *Nature* 504: 287–290
- Fabiani FD, Renault TT, Peters B, Dietsche T, Gálvez EJC, Guse A, Freier K, Charpentier E, Strowig T, Franz-Wachtel M *et al* (2017) A flagellum-specific chaperone facilitates assembly of the core type III export apparatus of the bacterial flagellum. *PLoS Biol* 15: e2002267

- Fukumura T, Makino F, Dietsche T, Kinoshita M, Kato T, Wagner S, Namba K, Imada K, Minamino T (2017) Assembly and stoichiometry of the core structure of the bacterial flagellar type III export gate complex. *PLoS Biol* 15: e2002281
- Ghosal D, Jeong KC, Chang Y-W, Gyore J, Teng L, Gardner A, Vogel JP, Jensen GJ (2019) Molecular architecture, polar targeting and biogenesis of the Legionella Dot/Icm T4SS. *Nat Microbiol* 4: 1173–1182
- Gilbreath JJ, Cody WL, Merrell DS, Hendrixson DR (2011) Change Is Good: variations in common biological mechanisms in the epsilon/proteobacterial genera *Campylobacter* and *Helicobacter*. *Microbiol Mol Biol Rev* 75: 84–132
- Godessart P, Lannoy A, Dieu M, Van der Verren SE, Soumillon P, Collet J-F, Remaut H, Renard P, De Bolle X (2020) β -Barrels covalently link peptidoglycan and the outer membrane in the α -proteobacterium *Brucella abortus*. *Nat Microbiol* 6, 27–33
- Guse A, Rohde M, Erhardt M (2020). Controlling minimal and maximal hook-length of the bacterial flagellum (Microbiology). *bioRxiv* <https://doi.org/10.1101/2020.03.25.007062> [PREPRINT]
- Hagen WJH, Wan W, Briggs JAG (2017) Implementation of a cryo-electron tomography tilt-scheme optimized for high resolution subtomogram averaging. *J Struct Biol* 197: 191–198
- Henderson LD, Matthews-Palmer TRS, Gulbranson CJ, Ribardo DA, Beeby M, Hendrixson DR (2020) Diversification of *Campylobacter jejuni* flagellar C-ring composition impacts its structure and function in motility, flagellar assembly, and cellular processes. *MBio* 11, e02286-19
- Hughes KT (2017) Flagellum length control: how long is long enough? *Curr Biol* 27: R413–R415
- Ito M, Takahashi Y (2017) Nonconventional cation-coupled flagellar motors derived from the alkaliphilic *Bacillus* and *Paenibacillus* species. *Extremophiles* 21: 3–14
- Johnson S, Fong YH, Deme JC, Furlong EJ, Kuhlen L, Lea SM (2020) Symmetry mismatch in the MS-ring of the bacterial flagellar rotor explains the structural coordination of secretion and rotation. *Nat Microbiol* 5: 966–975
- Johnson S, Furlong EJ, Deme JC, Nord AL, Caesar JJE, Chevance FFV, Berry RM, Hughes KT, Lea SM (2021) Molecular structure of the intact bacterial flagellar basal body. *Nat Microbiol* 6: 712–721
- Jones CJ, Macnab RM (1990) Flagellar assembly in *Salmonella typhimurium*: analysis with temperature-sensitive mutants. *J Bacteriol* 172: 1327–1339
- Joslin SN, Hendrixson DR (2009) Activation of the *Campylobacter jejuni* FlgSR two-component system is linked to the Flagellar export apparatus. *J Bacteriol* 191: 2656–2667
- Kaplan M, Ghosal D, Subramanian P, Oikonomou CM, Kjaer A, Pirbadian S, Ortega DR, Briegel A, El-Naggar MY, Jensen GJ (2019a) The presence and absence of periplasmic rings in bacterial flagellar motors correlates with stator type. *eLife* 8: e43487
- Kaplan M, Subramanian P, Ghosal D, Oikonomou CM, Pirbadian S, Starwalt-Lee R, Mageswaran SK, Ortega DR, Galnick JA, El-Naggar MY et al (2019b). *In situ* imaging of the bacterial flagellar motor disassembly and assembly processes. *EMBO J* 38: e100957
- Kaplan M, Sweredoski MJ, Rodrigues JPGLM, Tocheva EI, Chang Y-W, Ortega DR, Beeby M, Jensen GJ (2020) Bacterial flagellar motor PL-ring disassembly subcomplexes are widespread and ancient. *Proc Natl Acad Sci U S A* 117: 8941–8947
- Kawamoto A, Miyata T, Makino F, Kinoshita M, Minamino T, Imada K, Kato T, Namba K (2021) Native flagellar MS ring is formed by 34 subunits with 23-fold and 11-fold subsymmetries. *Nat Commun* 12: 4223
- Kodera N, Uchida K, Ando T, Aizawa S-I (2015) Two-ball structure of the flagellar hook-length control protein FliK as revealed by high-speed atomic force microscopy. *J Mol Biol* 427: 406–414
- Kremer JR, Mastronarde DN, McIntosh JR (1996) Computer visualization of three-dimensional image data using IMOD. *J Struct Biol* 116: 71–76
- Kubori T, Shimamoto N, Yamaguchi S, Namba K, Aizawa S-I (1992) Morphological pathway of flagellar assembly in *Salmonella typhimurium*. *J Mol Biol* 226: 433–446
- Kuhlen L, Abrusci P, Johnson S, Gault J, Deme J, Caesar J, Dietsche T, Mebrhatu MT, Ganief T, Macek B et al (2018) Structure of the core of the type III secretion system export apparatus. *Nat Struct Mol Biol* 25: 583–590
- Lee LK, Ginsburg MA, Crovace C, Donohoe M, Stock D (2010) Structure of the torque ring of the flagellar motor and the molecular basis for rotational switching. *Nature* 466: 996–1000
- Lele PP, Hosu BG, Berg HC (2013) Dynamics of mechanosensing in the bacterial flagellar motor. *Proc Natl Acad Sci U S A* 110: 11839–11844
- Lertsethtakarn P, Ottemann KM, Hendrixson DR (2011) Motility and Chemotaxis in *Campylobacter* and *Helicobacter*. *Annu Rev Microbiol* 65: 389–410
- Li H, Sourjik V (2011) Assembly and stability of flagellar motor in *Escherichia coli*: Flagellar motor assembly. *Mol Microbiol* 80: 886–899
- Liu R, Ochman H (2007) Stepwise formation of the bacterial flagellar system. *Proc Natl Acad Sci U S A* 104: 7116–7121
- Macnab RM (2003) How bacteria assemble flagella. *Annu Rev Microbiol* 57: 77–100
- Mastronarde DN (2005) Automated electron microscope tomography using robust prediction of specimen movements. *J Struct Biol* 152: 36–51
- Miller SI, Salama NR (2018) The gram-negative bacterial periplasm: size matters. *PLoS Biol* 16: e2004935
- Milne-Davies B, Wimmi S, Diepold A (2021) Adaptivity and dynamics in type III secretion systems. *Mol Microbiol* 115: 395–411
- Minamino T, Kawamoto A, Kinoshita M, Namba K (2020) Molecular organization and assembly of the export apparatus of Flagellar Type III secretion systems. *Curr Top Microbiol Immunol* 427: 91–107
- Nicastro D, Schwartz C, Pierson J, Gaudette R, Porter ME, McIntosh JR (2006) The molecular architecture of axonemes revealed by cryoelectron tomography. *Science* 313: 944–948
- Ortega DR, Oikonomou CM, Ding HJ, Rees-Lee P, Alexandria, Jensen GJ (2019) ETDB-Caltech: a blockchain-based distributed public database for electron tomography. *PLoS One* 14: e0215531
- Pettersen EF, Goddard TD, Huang CC, Couch GS, Greenblatt DM, Meng EC, Ferrin TE (2004) UCSF Chimera—a visualization system for exploratory research and analysis. *J Comput Chem* 25: 1605–1612
- Qin Z, Lin W, Zhu S, Franco AT, Liu J (2017) Imaging the motility and chemotaxis machineries in *Helicobacter pylori* by cryo-electron tomography. *J Bacteriol* 199: e00695-16
- Renault TT, Abraham AO, Bergmiller T, Paradis G, Rainville S, Charpentier E, Guet CC, Tu Y, Namba K, Keener JP et al (2017) Bacterial flagella grow through an injection-diffusion mechanism. *eLife* 6: e23136
- Renault TT, Guse A, Erhardt M (2019). Export mechanisms and energy transduction in type-III secretion machines. *Curr Top Microbiol Immunol* 427: 143–159
- Ribardo DA, Kelley BR, Johnson JG, Hendrixson DR (2019) A chaperone for the stator units of a bacterial flagellum. *MBio* 10: e01732-19
- Rossmann FM, Hug I, Sangermani M, Jenal U, Beeby M (2020) In situ structure of the *Caulobacter crescentus* flagellar motor and visualization of binding of a CheY-homolog. *Mol Microbiol* 114: 443–453

- Sandoz KM, Moore RA, Beare PA, Patel AV, Smith RE, Bern M, Hwang H, Cooper CJ, Priola SA, Parks JM et al (2021) β -Barrel proteins tether the outer membrane in many Gram-negative bacteria. *Nat Microbiol* 61: 19–26
- Santiveri M, Roa-Eguiara A, Kühne C, Wadhwa N, Hu H, Berg HC, Erhardt M, Taylor NMI (2020) Structure and function of stator units of the bacterial flagellar motor. *Cell* 183: 244–257.e16
- Shaffer CL, Gaddy JA, Loh JT, Johnson EM, Hill S, Hennig EE, McClain MS, McDonald WH, Cover TL (2011) *Helicobacter pylori* exploits a unique repertoire of type IV secretion system components for pilus assembly at the bacteria-host cell interface. *PLoS Pathog* 7: e1002237
- Tan J, Zhang X, Wang X, Xu C, Chang S, Wu H, Wang T, Liang H, Gao H, Zhou Y et al (2021) Structural basis of assembly and torque transmission of the bacterial flagellar motor. *Cell* 184: 2665–2679.e19
- Terahara N, Krulwich TA, Ito M (2008) Mutations alter the sodium versus proton use of a *Bacillus clausii* flagellar motor and confer dual ion use on *Bacillus subtilis* motors. *Proc Natl Acad Sci U S A* 105: 14359–14364
- Terahara N, Sano M, Ito M (2012) A bacillus flagellar motor that can use both Na⁺ and K⁺ as a coupling ion is converted by a single mutation to use only Na⁺. *PLoS One* 7: e46248
- Terashima H, Hirano K, Inoue Y, Tokano T, Kawamoto A, Kato T, Yamaguchi E, Namba K, Uchihashi T, Kojima S et al (2020) Assembly mechanism of a supramolecular MS-ring complex to initiate bacterial flagellar biogenesis in *Vibrio* species. *J Bacteriol* 202: e00236-20
- Thormann KM, Paulick A (2010) Tuning the flagellar motor. *Microbiology* 156: 1275–1283
- Tsang J, Hoover TR (2014) Requirement of the flagellar protein export apparatus component FliO for optimal expression of flagellar genes in *Helicobacter pylori*. *J Bacteriol* 196: 2709–2717
- Yamaguchi T, Makino F, Miyata T, Minamino T, Kato T, Namba K (2021) Structure of the molecular bushing of the bacterial flagellar motor. *Nat Commun* 12: 4469
- Zhao X, Norris SJ, Liu J (2014) Molecular architecture of the bacterial flagellar motor in cells. *Biochemistry* 53: 4323–4333
- Zhao X, Zhang K, Boquoi T, Hu B, Motaleb MA, Miller KA, James ME, Charon NW, Manson MD, Norris SJ et al (2013) Cryoelectron tomography reveals the sequential assembly of bacterial flagella in *Borrelia burgdorferi*. *Proc Natl Acad Sci U S A* 110: 14390–14395
- Zheng SQ, Keszthelyi B, Branlund E, Lyle JM, Braunfeld MB, Sedat JW, Agard DA (2007) UCSF tomography: an integrated software suite for real-time electron microscopic tomographic data collection, alignment, and reconstruction. *J Struct Biol* 157: 138–147
- Zhu S, Schniederberend M, Zhitnitsky D, Jain R, Galán JE, Kazmierczak BI, Liu J (2019) *In situ* structures of polar and lateral flagella revealed by cryo-electron tomography. *J Bacteriol* 201: e00117-19